In Vitro Conversion of Mammalian Prion Protein into Amyloid Fibrils Displays Unusual Features†

Ilia V. Baskakov*,‡,§ and Olga V. Bocharova‡

Medical Biotechnology Center, University of Maryland Biotechnology Institute, Baltimore, Maryland 21201, and Department of Biochemistry and Molecular Biology, University of Maryland School of Medicine, Baltimore, Maryland 21201

Received August 5, 2004; Revised Manuscript Received November 30, 2004

ABSTRACT: The "protein only" hypothesis of prion propagation postulates that the abnormal isoform of the prion protein, PrP^{Sc}, acts as a causative and transmissible agent of prion disease. In attempt to reconstitute prion infectivity in vitro, we previously developed a cell-free conversion protocol for generating amyloid fibrils from a recombinant prion protein encompassing residues 89−231 (rPrP 89−230) [Baskakov et al. (2002) *J. Biol. Chem. 277*, 21140]. When inoculated into transgenic mice, these amyloid fibrils induced prion disease, which can be efficiently transmitted to both wild-type and transgenic mice [Legname et al. (2004) *Science 305*, 673]. Here we show that the polymerization of rPrPs into the fibrils displays a number of distinctive kinetic features that are not typical for polymerization by other amyloidogenic polypeptides. Specifically, the lag phase of polymerization showed only modest dependence on protein concentration, and the conversion reaction displayed a dramatic volume-dependent threshold effect. To explain these unique kinetic features, we proposed that the conversion reaction is regulated by the dynamics between the rates of multiplication and deactivation of self-propagating fibrillar isoforms. Our further studies demonstrated that surface-dependent sorption of fibrillar isoforms is responsible for their deactivation in vitro, while fibril fragmentation seems to account for the multiplication of the active centers of polymerization. Our findings support the hypothesis that development of prion disease is controlled by a fine dynamic balance between self-propagation and clearance/deactivation of PrP^{Sc}.

The "protein only" hypothesis of prion propagation postulates that the abnormal isoform of the prion protein, PrP^{Sc},[1] acts as a causative and transmissible agent of the disease and propagates its pathological β-sheet-rich conformation in an autocatalytic manner (*1*). Conversion from PrP^{C} to PrP^{Sc} involves a substantial conformational change: PrP^{C} is a proteinase K- (PK-) sensitive α-helical monomer, whereas PrP^{Sc} is an multimer characterized by enhanced resistance toward PK digestion and increased amount of β-structure (*2*, *3*). Despite substantial differences between PrP^{C} and PrP^{Sc}, it is still unclear what physical properties can be used as a valid probe for monitoring generation of infectious PrP^{Sc} in vitro. It has been shown that prion disease can be transmitted in the absence of the PK-resistant form of PrP (*4*−*6*). On the other hand, generation of PK-resistant PrP in vitro did not correlate with amplification of infectivity (*7*−*9*). The fact that PrP^{Sc} exists in multiple forms referred to as strains and subtypes, which are characterized by a broad range of PK resistance and diverse physical properties (*10*−*16*), creates additional challenges for reconstitution of prion infectivity in vitro. Notably, cell-free conversions of recombinant PrPs produced a large diversity of abnormal β-sheet-rich isoforms, many of which possess some but not all PrP^{Sc}-like properties (*8*, *17*−*24*). However, despite broad conformational diversity of these isoforms, reconstitution of the infectious form of PrP has been difficult to achieve (*25*). Since no physical property has been identified as an exclusive feature of infectious PrP^{Sc}, the ability of PrP^{Sc} to propagate itself in an autocatalytic manner seems to be the key element to follow in reconstitution of infectivity in vitro.

In one of our previous studies using mouse recombinant PrP encompassing residues 89−230 (Mo rPrP 89−230), we developed an in vitro conversion protocol that generates self-propagating amyloid isoforms of rPrP 89−231 (*26*). The cell-free conversion of rPrP displayed a species barrier, an important attribute of prion propagation (*27*). When inoculated into transgenic mice expressing only PrP 89−230, this self-propagating isoform of Mo rPrP 89−231 induced prion disease that could be efficiently transmitted to both wild-type and transgenic mice (*28*). Our two studies provided strong evidence for the "protein only" hypothesis of prion propagation in mammals and introduced the simplest biologically relevant in vitro conversion system developed so far that can be used to study the biophysical mechanism of prion replication.

In the present study we tested the extent to which the kinetics of in vitro conversion of PrP follows the nucleation−

† This work was supported by National Institute of Health Grant NS045585 to I.V.B.

* To whom correspondence should be addressed: 725 W. Lombard St., Baltimore, MD 21201. Phone 410-706-4562; fax 410-706-8184; e-mail Baskakov@umbi.umd.edu.

‡ Medical Biotechnology Center, University of Maryland Biotechnology Institute.

§ Department of Biochemistry and Molecular Biology, University of Maryland School of Medicine.

[1] Abbreviations: PrP, prion protein; rPrP, recombinant prion protein; PrP^{C}, cellular isoform of the prion protein; PrP^{Sc}, disease associated isoform of the prion protein; NPM, nucleation−polymerization mechanism; Hu, human; Mo, mouse; SHa, Syrian hamster; ThT, thioflavin T; PK, proteinase K; GdnHCl, guanidine hydrochloride; FTIR, Fourier transform infrared spectroscopy.

10.1021/bi048322t CCC: $30.25
Published on Web 02/01/2005

polymerization mechanism (NPM) (*29*). NPM was originally introduced in 1975 to describe polymerization of proteins (*30*) and has been later applied to amyloid formation (*29*). For the last several years NPM was used broadly for modeling a complex mechanism of fibril polymerization, in which a variety of amyloidogenic proteins and prions are involved (*29*, *31*−*35*).

In the present study two recombinant PrPs were used: truncated PrP encompassing residues 90−231 (rPrP 90−231) and full-length PrP encompassing residues 23−230 (rPrP 23−230). Using both PrPs, we found that the lag phase of the in vitro conversion showed modest dependence on protein concentrations. On the other hand, the cell-free conversion reaction displayed a dramatic volume-dependent threshold effect. We present evidence that fragmentation of fibrils may account for the multiplication of the active centers of polymerization, while surface-dependent sorption of self-propagating fibrillar isoforms to tube walls is responsible for the deactivation. Taken together, our data on the kinetics of polymerization were consistent with the nucleation polymerization model, which postulates that in addition to the nucleation and elongation steps, there is a multiplication of active centers of propagation occurring in parallel with their deactivation. According to this model, dynamic equilibrium between multiplication and deactivation of the active centers regulates the rate of conversion. Our findings support the hypothesis that prion replication is a dynamic process controlled by a fine balance between self-propagation and clearance of PrP^{Sc} (*36*).

MATERIALS AND METHODS

Protein Expression and Purification. Recombinant mouse (Mo), human (Hu), and Syrian hamster (SHa) truncated PrPs were purified as previously described (*27*). Mouse PrP 23−231 DNA was polymerase chain reaction- (PCR-) amplified from pcDNA3 plasmids containing the full-length PrP gene, inserted into pET101/D-TOPO vector (Invitrogen), and transformed into Top10 cells (Invitrogen). The transformants were tested by PCR amplification, and the DNAs from the positive clones were checked by DNA sequencing and retransformed into BL21 (DE3) Star cells (Invitrogen). For expression, transformants were inoculated into 10 mL of Luria−Bertani (LB)/carbenicillin medium (0.1 mg/mL carbenicillin) and were grown at 37 °C for 3.5 h. The entire culture was inoculated into 100 mL of LB/carbenicillin medium and grown overnight (∼16 h). A portion (5%) of the overnight culture was inoculated into Terrific Broth (TB) medium (300 mL) supplemented with carbenicillin (0.1 mg/mL) and grown at 37 °C until the A_{600nm} reached 0.6. Expression was induced by addition of isopropyl β-D-thiogalactopyranoside (Sigma) to a final concentration of 1 mM, and the cultures were grown for an additional 5 h. Cells were harvested by centrifugation, resuspended in lysis buffer [50 mM Tris, 1 mM ethylenediaminetetraacetic acid (EDTA), and 100 mM NaCl, pH 8; 9 mL/g of pellet], followed by the addition of lysozyme (200 μg/mL) and phenylmethanesulfonyl fluoride (PMSF) (20 μg/mL) with subsequent incubation on ice for 20−40 min. Deoxycholic acid (1 mg/mL) was added, followed by incubation on ice for 20−30 min, subsequent addition of DNase (10 μg/mL), and a final incubation for 30−45 min. The lysate was centrifuged at 20000*g* for 20 min. The resulting pellet was dissolved in IMAC buffer A (5 mL/g of pellet; 0.1 M Na_2HPO_4, 10 mM Tris, 8 M urea, and 10 mM β-mercaptoethanol, pH 8), incubated for 2 h at room temperature, and centrifuged at 20000*g* for 15 min to remove insoluble material. The solubilized inclusion bodies were incubated with nitrilotriacetic acid (NTA) fast-flow Sepharose resin (Amersham Biosciences, Sweden) precharged with Ni ions at room temperature for 1 h in a top−bottom mixer. The NTA column was washed with five volumes of IMAC buffer A, followed by elution of rPrP in IMAC buffer B (0.1 M Na_2HPO_4, 10 mM Tris, 8 M urea, and 10 mM β-mercaptoethanol, pH 4.5). Fractions containing rPrP were diluted to a final protein concentration of 0.5 mg/mL with 9 M urea in 0.1 M Tris buffer, pH 8.0, and dialyzed against 9 M urea in 0.1 M Tris buffer, pH 8.0, to eliminate β-mercaptoethanol. The dialyzed solution was diluted 3-fold with buffer I (0.1% trifluoroacetic acid/H_2O), loaded on a 25 mm × 25 cm C4 HPLC column (Vydac), and eluted with a gradient of buffer II (0.1% trifluoroacetic acid/acetonitrile). Fractions containing rPrP were eluted in 40% acetonitrile and lyophilized. The purity of final rPrP preparation was confirmed by sodium dodecyl sulfate−polyacrylamide gel electrophoresis (SDS−PAGE) followed by silver staining and electrospray mass spectrometry to be a single species with an intact disulfide bond. Ten milligrams of 99.5+% pure rPrP was obtained per liter of culture.

In Vitro Conversion of rPrPs into Amyloid Fibrils. To form amyloid fibrils, a stock solution of rPrP in 6 M GdnHCl was diluted to a final protein concentration of 0.1−50 μM in the presence of 1 M GdnHCl, 2.4 M urea, and 150 mM NaCl and incubated at 37 °C in conical plastic tubes (Eppendorf) with continuous shaking at 600 rpm on a Delfia plate shaker (Wallac). The conversion reactions at pH 5.0 were carried out in 20 mM sodium acetate buffer and at pH 6.8 in phosphate-buffered saline (PBS). When the reaction was carried out under the same solvent conditions but in a reaction volume <0.3 mL, the conversion did not occur spontaneously. However, it was possible to induce the conversion by seeding. The conversion in reaction volume <0.3 mL is referred to as subthreshold conditions.

The kinetics of fibril formation was monitored by a ThT-binding assay. Aliquots (4 μL unless specified) withdrawn during the time course of incubation at 37 °C were diluted into 5 mM sodium acetate buffer (pH 5.5) to a final concentration of rPrP of 0.3 μM (unless specified), and then ThT (Invitrogen, Carlsbad, CA) was added to the final concentration of 10 μM. Six emission spectra (from 460 to 520 nm) were recorded for each sample in 0.4 cm rectangular cuvettes with excitation at 445 nm on a FluoroMax-3 fluorometer (Jobin Yvon, Edison, NJ); both excitation and emission slits were 4 nm. Spectra were averaged and the fluorescence intensity at emission maximum (482 nm) was determined.

Congo Red Staining. Plastic tubes were rinsed with phosphate-buffered saline (PBS) followed by incubation with freshly filtered aqueous solution of Congo red (50 μM) for 30 min on a rotary shaker. To remove amyloid fibrils from tube walls, sarcosyl was added to a final concentration of 2% and tubes were treated by ultrasound for 1 min in a Branson 2510 ultrasonic cleaners bath (Danbury, CT).

FTIR Spectroscopy. FTIR spectra were measured with a Bruker Tensor 27 FTIR instrument (Bruker Optics, Billerica,

MA) equipped with a mercury−cadmium−telluride (MCT) detector cooled with liquid nitrogen. Samples of rPrP were dialyzed against 10 mM sodium acetate buffer, pH 5.0, and 10 μL of each isoform (0.5 mg/mL for the amyloid fibrils or 3 mg/mL for the α-rPrP) was loaded into BioATRcell II. A total of 128 scans at 2 cm^{-1} resolution were collected for each sample under constant purging with nitrogen; a correction for water vapor was applied, and background spectra of water were subtracted.

Fluorescent Imaging of Fibrils. Fluorescence microscopy experiments were carried out on an inverted microscope (Nikon Eclipse TE2000-U) with illumination system X-Cite 120 (EXFO Photonics Solutions Inc.) connected through fiber-optics with a 1.3 aperture Plan Fluor 100× NA objective. The emission was isolated from Rayleigh and Raman-shifted light by a combination of filters: an excitation filter 485DF22, a beam splitter 505DRLPO2, and an emission filter 510LP (Omega Optical, Inc.). Digital images were acquired by use of a cooled 12-bit CoolSnap HQ charge-coupled device (CCD) camera (Photometrics). Prior to imaging, fibrils were diluted to a final concentration of rPrP equivalent to 0.1 μM in 10 mM sodium acetate buffer and stained with ThT (10 μM) for 3 min. Fibril length was calculated by an automated measurement routine with V++ software version 4.0 (Auckland, New Zeland).

Negative Staining and Electron Microscopy. Negative staining was performed on carbon-coated 400-mesh copper grids that were glow-discharged prior to staining. The samples were adsorbed for 30 s, stained with freshly filtered 2% ammonium molybdate, dried, and then viewed in a Zeiss EM 10 CA electron microscope.

RESULTS

According to the NPM, the rate-limiting step of polymerization is regulated by the formation of oligomeric nuclei; therefore, the length of the lag phase of spontaneous conversion is expected to depend dramatically on the concentration of polypeptide (*29*). To test whether the cell-free conversion follows the NPM, we analyzed the kinetics of nonseeded amyloid formation as a function of rPrP concentration. Using truncated human (Hu) rPrP 90−231, we observed very modest dependence of the lag phase on protein concentration (Figure 1A). Thus, an 8-fold increase in concentration resulted in reduction of the lag phase from 6 h at 6.2 μM to 4.5 h at 50 μM (Figure 1A). The kinetics of fibril formation of mouse (Mo) rPrP 89−230 and Syrian hamster (SHa) rPrP 90−231 varied with protein concentration in a very similar manner, displaying only modest dependence of the lag phase on concentration (data not shown). Therefore, weak concentration dependence of the lag phase is not limited to Hu rPrP 90−231 but rather is general for the in vitro conversion of rPrPs. The weak dependence of the lag phase is usually attributed to an accumulation of large off-pathway aggregates, which are in competition with on-pathway polymerization. However, at given experimental conditions (pH 6.8, partially denaturing concentrations of urea and GdnHCl), Hu rPrP 90−231 remains monomeric even after prolonged incubation at 37 °C (*27*).

The second step of amyloid formation referred to as elongation was accompanied by rapid growth of ThT fluorescence and displayed stronger dependence on protein concentration (Figure 1B). Our previous studies demonstrated that growth of ThT fluorescence correlated well with consumption of the monomeric species and that the ThT assay can be used as a valid probe for analysis of polymerization kinetics (*26*, *27*). To determine the reaction rate of the elongation, we employed an expression originally introduced by van't Hoff: $\log V = A + n \log C$, where V is the initial rate of elongation, C is the rPrP concentration, and n is the apparent reaction order. The slope of the plot ($n = 0.93 \pm 0.09$) shows that the elongation may follow apparent first-order kinetics. The first-order or less than first-order kinetics is consistent with the model in which the rate-limiting step of polymerization is controlled by conformational rearrangement of polypeptides upon their binding to fibrillar ends rather than the binding step itself (Figure 8).

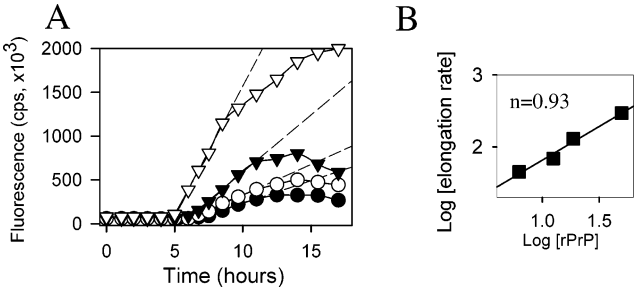

FIGURE 1: (A) Kinetics of Hu rPrP 90−231 conversion into the amyloid form monitored by ThT-binding assay and measured for different concentrations of rPrP: 50 μM (▽), 20 μM (▼), 12.5 μM (○), 6.2 μM (●). Dashed lines represent the initial rates of elongation and are extrapolated below the detection limit of the ThT assay. Generation of the amyloid fibrils was carried out at 37 °C in PBS (pH 6.8), 1 M GdnHCl, and 2.4 M urea in a reaction volume of 0.8 mL. Aliquots (4 μL) were withdrawn in the time course of the reaction and diluted 80-fold to final concentrations of rPrP 0.625, 0.25, 0.16, and 0.08 μM, respectivly, for the ThT-binding assay. (B) van't Hoff plot of the initial rate of elongation as a function of rPrP concentration. The range of rPrP concentrations used in the plot is between 6.2 and 50 μM. The slope of the plot ($n = 0.93 \pm 0.09$) represents the apparent reaction order of the elongation reaction.

Because full-length recombinant PrP that encompasses residues 23−230 (rPrP 23−230) represents a more relevant biological model, we set out to determine whether the lag phase of Mo rPrP 23−230 polymerization also displays a weak dependence on protein concentration. To our surprise, here we found that a decrease of rPrP 23−230 concentrations from 22 to 4.4 μM resulted in a reduction of the lag phase from 2 h to 1 h (Figure 2A). Further decrease of the concentration to 1.1 μM did not change the length of the lag phase. Shortening of the lag phase upon a decrease in rPrP 23−230 concentration indicates that significant off-pathway aggregation of rPrP may interfere with the polymerization reaction. Other amyloidogenic proteins prone to nonspecific aggregation have been also shown to display atypical dependence of the lag phase on protein concentration (*32*, *37*, *38*). Using electron microscopy, we observed substantial amount of nonfibrillar aggregates coexisting together with amyloid fibrils when the polymerization reaction was carried out at high concentrations of protein (Figure 2C, left panel). When the conversion reactions were carried out at protein concentrations 5 μM or less, predominantly fibrillar structures were seen by electron microscopy (Figure 2C, right panel). Concentration-dependent off-

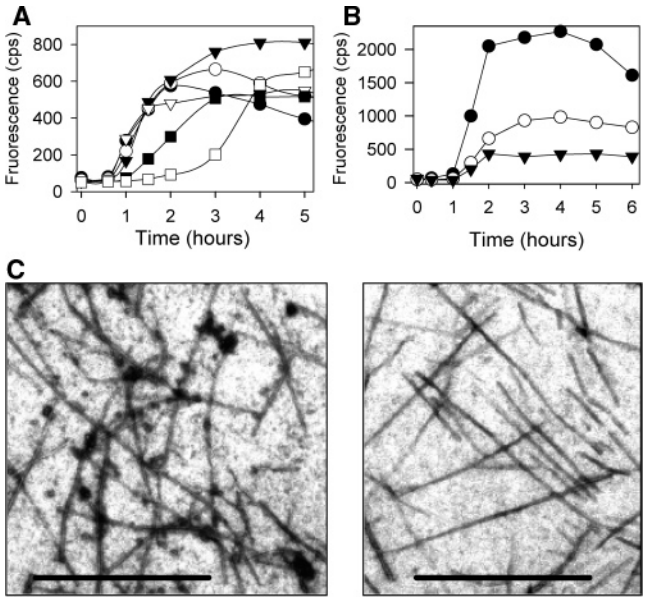

FIGURE 2: (A) Kinetics of amyloid formation of Mo rPrP 23−230 measured for different concentrations of rPrP: 22 μM (□), 11 μM (■), 4.4 μM (▽), 3.3 μM (▼), 2.2 μM (○), 1.1 μM (●). Aliquots were withdrawn in the time course of the reaction and diluted to the final concentration of rPrP 0.3 μM for ThT-binding assay. The volume of aliquots was variable (4−80 μL) depending on the initial concentration of rPrP. To reduce the effect of withdrawing aliquots on the reaction volume, multiple samples were started in parallel for the reactions carried at concentrations below 11 μM and aliquots were taken from different samples at each time point. By the end of measurements the reaction volume was reduced less than 20% in each sample. The initial reaction volume was 0.9 mL. (B) Kinetics of amyloid formation monitored in the presence of ThT (10 μM) for different concentrations of Mo rPrP 23−230: 1.1 μM (●), 0.44 μM (○), and 0.22 μM (▼). Formation of fibrils at lowest concentration of 0.22 μM was confirmed by fluorescent microscopy. Formation of the amyloid fibrils presented in panels A and B was carried out at 37 °C in PBS (pH 6.8), 1 M GdnHCl, and 3 M urea. (C) Electron micrographs of negatively stained amyloid fibrils formed at concentrations of rPrP 22 μM (left panel) and 4.4 μM (right panel). Nonfibrillar aggregates are formed together with fibrils at concentration 22 μM. The size of the scale bars is 1 μm.

pathway aggregation of rPrP 23−230 is consistent with recent studies that demonstrated that nonspecific aggregation of full-length rPrP occurs at neutral pH and is facilitated in the presence of salt (*39*). Because nonspecific aggregation is triggered by deprotonation of His side chains within the N-terminal domain 23−91, the full-length rPrP has much higher propensity for aggregation than rPrP 90−231.

To test whether the amyloid fibrils can be generated at concentrations of rPrP below 1.1 μM, we carried out the conversion reactions without taking out aliquots in the presence of ThT. This allowed us to monitor the kinetics at the protein concentrations below 1 μM (Figure 2B). Remarkably, we observed amyloid formation even at the lowest concentration of rPrP tested (0.22 μM) without any substantial increase in the lag phase (Figure 2B). This concentration was approximately 2000-fold lower than that reported for nucleation-dependent polymerization of PrP-derived peptides (*40*). Our data demonstrate the lag phase of amyloid formation of both truncated and full-length rPrPs shows weak dependence on protein concentration. Furthermore, we found that the in vitro conversion of rPrP 23−230 can be achieved at very low concentrations.

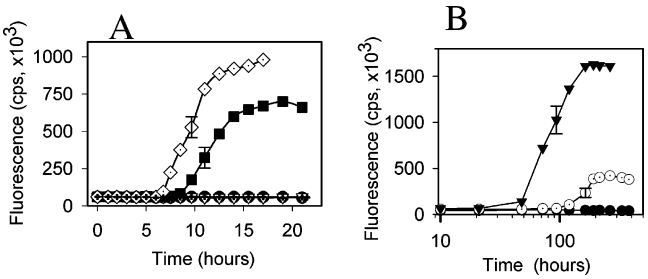

FIGURE 3: (A) Kinetics of amyloid formation of Hu rPrP 90−231 (24 μM, in PBS, pH 6.8, 1 M GdnHCl, and 2.4 M urea) as a function of the reaction volume: 0.5 mL (◇), 0.4 mL (■), 0.3 mL (▽), 0.2 mL (●), and 0.1 mL (+). (B) Kinetics of amyloid formation of SHa rPrP 90−231 (16 μM, in 20 mM sodium acetate buffer at pH 5.0, 1 M GdnHCl, 2.4 M urea, and 150 mM NaCl) as a function of the reaction volume: 1.2 mL (▼), 0.4 mL (○), and 0.1 mL (●). Error bars represent standard deviations for triplicates. Aliquots (4 μL) were withdrawn in the time course of the reaction and diluted to a final concentration of rPrP 0.3 μM for the ThT-binding assay. To reduce the effect of withdrawing aliquots on the reaction volume, multiple samples were started in parallel for the reactions carried out in 0.1 and 0.2 mL, and 4 μL aliquots were taken from different samples at each time point. By the end of measurements the reaction volume was reduced less than 20% in each sample.

While studying the kinetics of fibril formation, we were surprised to discover that other factors contribute more substantially in determining the length of the lag phase than the protein concentration. In particular, we found that polymerization into amyloid fibrils was very sensitive to reaction volume. Specifically, the decrease of the reaction volume carried out in conical plastic tubes (1.5 mL Eppendorfs) from 0.5 mL to 0.4 mL resulted in longer lag phase, slower rate, and lower yield of fibril formation of Hu rPrP 90−231 (Figure 3A). SHa rPrP 90−231 and Mo rPrP 89−230 also showed strong dependency of the reaction rate and the lag phase on the reaction volume. For instance, the reduction of the reaction volume from 1.2 to 0.4 mL resulted in a 50-h longer lag phase for SHa rPrP 90−231 (Figure 3B). Furthermore, we observed a dramatic threshold effect upon the gradual decrease of the reaction volume. The conversion of Hu rPrP 90−231 occurred only in samples with the reaction volume exceeding 0.3 mL, while samples with a reaction volume below 0.3 mL did not show any fibrils even after prolonged incubation as judged by ThT binding assay (Figure 3A). Similarly, by decreasing the reaction volume of SHa rPrP 90−231 to under 0.3 mL, the polymerization reaction was completely abolished (Figure 3B). The in vitro conversion of Mo rPrP 89−231 displayed similar volume-dependent effects (data not shown).

We noticed that the decrease in reaction volume to under 0.3 mL substantially reduces the effectiveness of shaking, which seems to be linked to fibril fragmentation and formation of new active centers (*41*). A decrease in reaction volume is also equivalent to an increase in surface-to-volume ratio. Vessel surfaces may either facilitate the formation of new nucleation centers (*42*) or deactivate existing ones, thus having a significant impact on the lag phase and final yield of the reactions. In our case, the observation of an apparent volume-dependent threshold is consistent with the scenario that self-propagating isoforms of rPrP are adsorbed and deactivated by the vessel surfaces. As the reaction volume decreases, the surface-to-volume ratio grows. Therefore, one can hypothesize that the threshold may be observed when

the rate of surface-dependent deactivation exceeds the rate of multiplication of self-propagating isoforms.

To test this hypothesis, first, we sought to elucidate whether self-propagating amyloid isoforms of rPrP are adsorbed to the surface of the plastic tube during the conversion process. To test this we used the amyloid-specific dye Congo red that has been exploited widely to stain amyloid deposits in vitro and in vivo (*43*). The plastic tubes used for the in vitro conversion of Hu rPrP 90−231 were rinsed with PBS and incubated with Congo red. We found that only those tubes that were used for the conversion reactions bound Congo red (Figure 4A, tube 2). Binding of the dye to tube walls was accompanied by a shift of Congo red color from orange to pink, a change that usually accompanies staining of amyloid-specific structures. Ultrasound treatment of plastic tubes for 1 min in the presence of 2% sarcosyl removed amyloid deposits from the tube walls (Figure 4A, tube 3). rPrP deposits removed from the walls showed birefringence under polarized light, an indication of amyloid-specific structure (data not shown). The FTIR spectra of rPrP deposits showed a major band at 1622 cm^{-1} and a minor broad band centered at 1535 cm^{-1}; both are characteristic of β-sheet structures with intermolecular hydrogen bonds. A smaller band at 1693 cm^{-1} was indicative of antiparallel β-sheets (Figure 4B,C, —). These spectra were substantially different from that of the α-monomer (Figure 4B,C, − − −), which displayed major bands at 1651 and 1550 cm^{-1}, a characteristic of α-helices. The increased tendency of amyloid forms for binding to tube walls was not limited to Hu rPrP 90−231. We found that self-propagating amyloid isoforms of rPrPs of all species tested (Mo, Hu, and SHa) bind well to walls of plastic tubes during the conversion reaction. Furthermore, both plastic and glass surfaces showed high propensity to retain amyloid deposits regardless whether these surfaces were siliconated or not. The propensity of amyloid isoforms of rPrP for binding to various materials is reminiscent of that of PrP^{Sc}. It is known that prion diseases can be efficiently transmitted through wires and surgical instruments contaminated with PrP^{Sc} (*44*−*47*). Our data confirmed that the amyloid of rPrP has a high tendency of sorption to walls of reaction vessels.

The surface-dependent deactivation seems to be one of the possible factors that may shift a balance between deactivation and generation of new active centers. One may hypothesize that the reaction can be stimulated even at unfavorable surface-to-volume ratio by adding seeds. Therefore, we were interested in testing whether the conversion reaction can be induced by exogenous addition of amyloid fibrils at subthreshold conditions. We seeded the fresh reaction carried out in a reaction volume of 0.3 mL with preformed fibrils. While no fibril formation was detected in solution in the absence of seeding, addition of small amount of seeds (0.1−2% w/w) initiated the conversion (Figure 5A). Notably, while the length of the lag phase was dependent on the amount of seeds added, the initial velocity measured as a growth of ThT fluorescence was independent of the amount of seeds. According to the NPM, exogenous addition of seeds bypasses the formation of nucleus, which is the rate-limiting step of the polymerization (*29*). If the seeded conversion under subthreshold conditions represents mainly an elongation of original seeds, than the rate of conversion should be proportional to the amount of seeds added to the

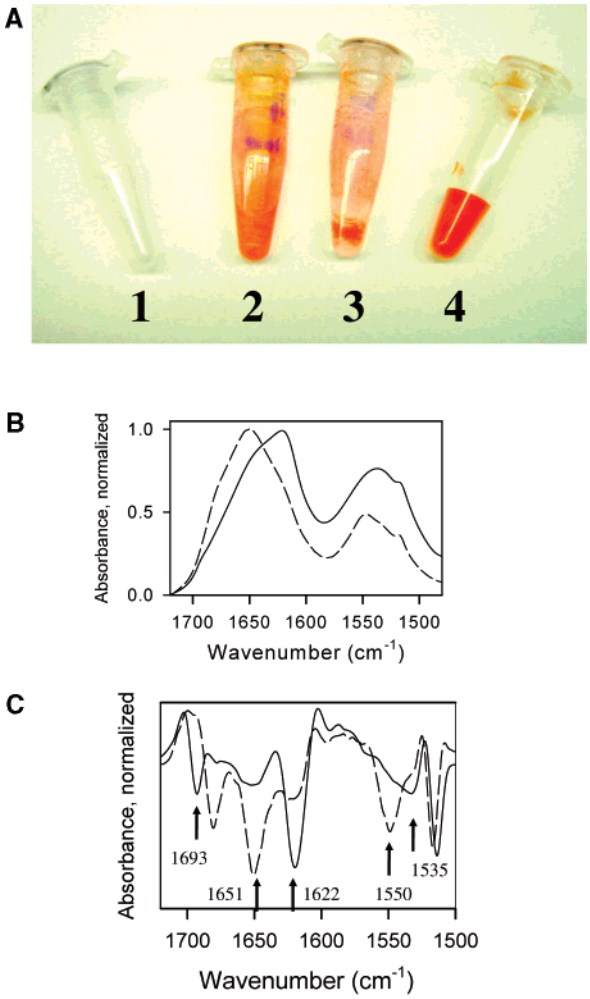

FIGURE 4: (A) Amyloid isoforms adsorb to walls of plastic tubes. The plastic tubes used for the in vitro conversion of Hu rPrP 90−231 (24 μM, in PBS, pH 6.8, 1 M GdnHCl, and 2.4 M urea, reaction volume 0.9 mL) were washed with PBS (tube 1), stained with Congo red (50 μM) for 30 min (tube 2), and incubated in an ultrasonic bath for 1 min in the presence of 2% sarcosyl (tube 3). An unused tube incubated with Congo red does not show any staining (tube 4). (B) FTIR spectrum of Hu rPrP 90−231 removed from the tube walls (—). The FTIR spectrum of Hu rPrP 90−231 in predominantly α-monomeric form (90% α-rPrP) is given for comparison (− − −). Both samples were dialyzed against 10 mM sodium acetate buffer, pH 5.0, before the FTIR measurement. The sample of Hu rPrP 90−231 in predominantly α-monomeric form contained approximately 10% β-oligomer, as assessed by size-exclusion chromatography (*65*). Formation of the β-oligomer normally occurs at high concentration of rPrP 90−231 (3 mg/mL), which was required for FTIR measurements. The shoulder displayed by predominantly α-monomeric sample at 1622 cm^{-1} is due to presence of the β-oligomeric species. (C) Second derivatives of FTIR spectra in the amide I and II regions. The line definitions are the same as for panel B.

reaction mixture. Accordingly, the slope of the polymerization kinetics is expected to be proportional to the amount of seeds (Figure 5B). Instead, we found that the rate of seeded polymerization was similar regardless of the amount of seeds added to the reaction. Furthermore, the seeded conversion also displayed a substantial lag phase, illustrating the complexity of seeded conversion. Overall, the present experiment demonstrated that the conversion reaction can be induced even under subthreshold conditions by seeding. However, the rate of the seeded polymerization was not determined entirely by the amount of catalytic centers

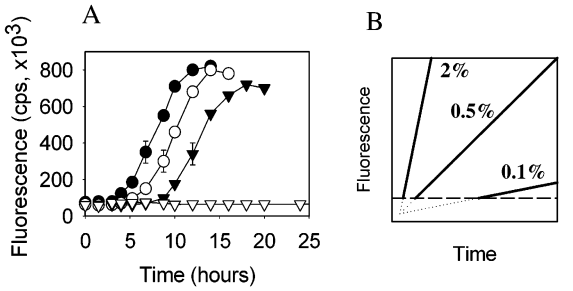

FIGURE 5: (A) Kinetics of amyloid formation of Hu rPrP 90−231 (24 μM) carried out at subthreshold conditions (in the reaction volume of 0.3 mL in PBS, pH 6.8, 1 M GdnHCl, and 2.4 M urea) induced by seeding with 0.1% (w/w) (▼), 0.5% (○), and 2% (●) preformed fibrils or without seeding (▽). Seeds are added to the fresh reaction mixture at time zero. Aliquots (4 μL) were withdrawn in the time course of the reaction and diluted to a final concentration of rPrP 0.3 μM for the ThT-binding assay. Error bars represent standard deviations for triplicates. (B) Theoretical kinetic curves representing seeded amyloid formation. According to the NPM, the slope of the kinetic curves is expected to be proportional to the amount of seeds added at time zero (*29*). In the absence of secondary nucleation, the kinetic curves in seeded conversion reflect only the process of linear elongation of fibrils. (− − −) Hypothetical detection limit of the assay; (•••) extrapolation of the kinetic curves below the detection limit. The conversion is not measurable at the initial stage due to detection limits; therefore the initial time intervals of conversion are often referred to as a lag phase. The NPM predicts that both the apparent lag phase and the rate of elongation are a function of the amount of seeds.

provided exogenously. Therefore, the rate-limiting step of elongation may not be dictated by the binding of polypeptides to fibrillar ends and/or their consequent rearrangement but rather determined by some yet unknown process.

Previous studies postulated that fragmentation of fibrils is an important step of polymerization and may account for highly cooperative kinetics of in vitro conversion (*41*, *48*, *49*). Indeed, the elongation reaction by itself does not generate new active centers, unless fibril fragmentation and/or fibril-dependent secondary nucleation occur. To gain insight into the mechanism of multiplication of the active centers, we monitored a change in length of fibrils in the time course of the conversion by epifluorescent microscopy (Figure 6). For this purpose, we used full-length Mo rPrP 23−230 at pH 5.0, because it forms fibrils that are long enough to be accurately measured. At pH 5.0 the fibrils of Mo rPrP 23−230 do not coaggregate and can be seen as single fibrils.

Using epifluorescent microscopy, we observed a large number of short fibrils by the end of the lag phase (Figure 6B, 17 h of incubation). Interestingly, while most fibrils were shorter than 0.25 μm, a small fraction (~5%) of relatively long fibrils (0.5−1 μm) can be seen even at the early elongation stage (17 h of incubation). Nevertheless, the histogram of fibrillar length at 17 h could be fitted with a single Gaussian distribution. Over time, the total number and the average length of fibrils increased (Figure 6B, 20 and 23 h of incubation). A broad distribution of fibrillar length becomes evident at 23 h, indicating that no discrete length but rather a continuum of fibrillar sizes existed. Starting at the 20 h time point the histogram could be fitted only with two Gaussian curves, while fitting with a single Gaussian was unsatisfactory. Notably, by the end of the elongation stage the fibrillar size distribution showed a subpopulation of short fibrils together with various fibrils of higher length

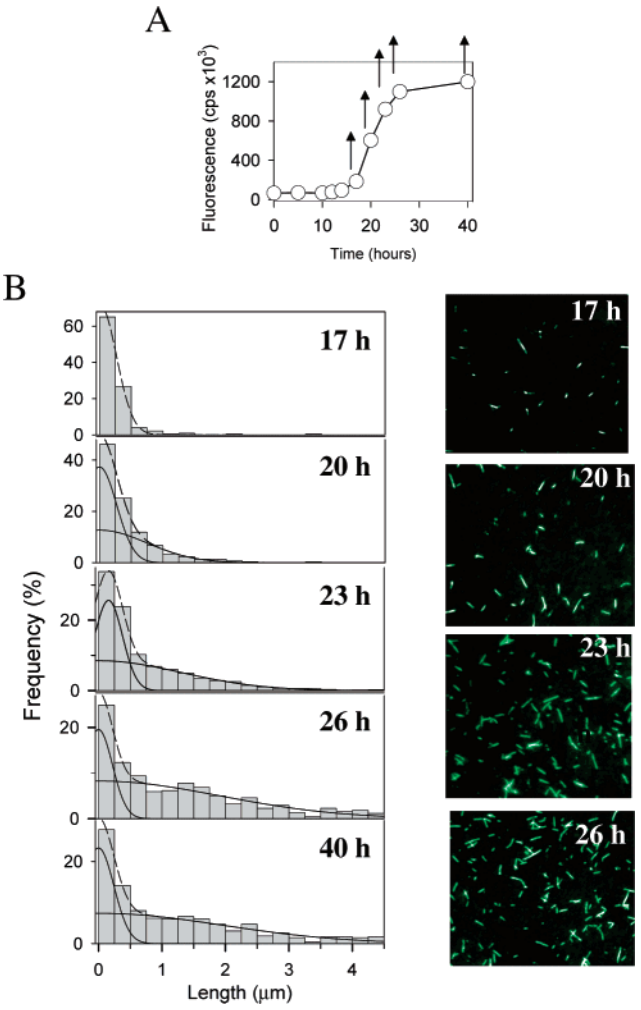

FIGURE 6: Fibril length distribution as a function of elongation time. **(**A) Kinetics of amyloid formation of Mo rPrP 23−230 (11 μM at 37 °C in 20 mM sodium acetate buffer at pH 5.0, 1 M GdnHCl, 3 M urea, and 150 mM NaCl, in a reaction volume of 0.6 mL) monitored by ThT-binding assay. In parallel with the ThT-binding assay, aliquots were withdrawn in the time course of the reaction and diluted to the final concentration of rPrP 0.1 μM for fluorescent imaging presented in panel B. Because amyloid fibrils have a tendency to coaggregate at neutral pH, this experiment was conducted at pH 5.0, which produces a much longer lag phase than pH 6.8. **(**B) Fibril length distribution and fluorescent images obtained at 17, 20, 23, 26, and 40 h of incubation at 37 °C. For each time point, the length distribution is based on measuring 1200 fibrils taken in 5−10 fields of view. (− − −) Fitting to either one or two Gaussian distributions; (—) individual Gaussian distributions.

(Figure 6B, 26 and 40 h of incubation). One may speculate that such broad distribution of fibrillar length is indicative of high heterogeneity of the elongation rate among individual fibrils. Although differences in the elongation rate may account in part for a broad distribution in fibrillar size, this explanation is not consistent with rapid overall kinetics of elongation as measured by the ThT assay. Surprisingly, a substantial fraction of fibrils (~30%) remained very short (<0.25 μM) even at the end of the elongation stage. There are two possible explanations for this observation. The process of fibril elongation may be terminated at an early stage, producing a subpopulation of short fibrils. Alternatively, fibrils may undergo fragmentation, a process that constantly occurs in parallel with elongation, resulting in a subpopulation of short fibrils. The second hypothesis is consistent with the recent studies by Weissman and co-

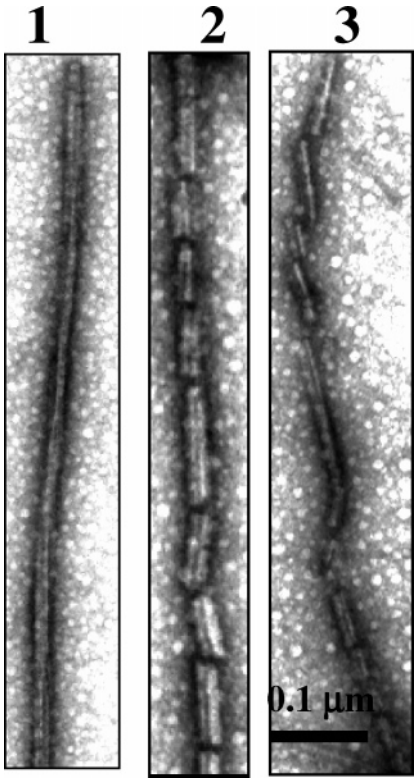

FIGURE 7: Electron micrographs of negatively stained amyloid fibrils of Mo rPrP 23−230: an intact fibril (panel 1) and fragmented fibrils (panels 2 and 3).

workers (*41*), who demonstrated that fragmentation of amyloid fibrils of yeast prion protein Sup 35 occurs in parallel with elongation and is caused by agitation. Interestingly, agitation did not affect the rate of binding of monomer to fibril ends; however, it accelerated polymerization by creating new active centers through fragmentation of Sup 35 fibrils. While Sup 35 was shown to be able to polymerize slowly even without agitation, we were unable to detect any amyloid fibrils of rPrP in test tubes without permanent shacking.

At this point, it is difficult to assess the role of fibril fragmentation and termination of elongation in generation of short fibrils. Nevertheless, by using electron microscopy we were able to see fragmented fibrils (Figure 7). Because fibrillar pieces remain aligned along the *Z*-axis, such fragmentation is believed to occur after attachment of each individual fibril to grids rather than in bulk solution. Although the type of fragmentation we observed is a result of sample preparation for electron microscopy, our observation emphasizes an intrinsic propensity of the amyloid fibrils to break into short pieces despite their apparently rigid structure. The extent to which fibrillar fragmentation occurs in aqueous solution and factors affecting it remain to be determined.

DISCUSSION

In the present study, we demonstrated that the in vitro conversion of rPrP into amyloid fibrils displays several distinctive kinetic features: (1) the weak dependence of the lag phase on the concentration of rPrP; (2) apparent first-order kinetics of elongation; (3) the dramatic effect of the reaction volume on the length of the lag phase; (4) an

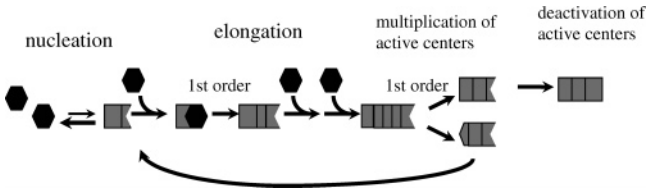

FIGURE 8: Schematic representation of rPrP polymerization. In addition to the steps of nucleation and elongation, the conversion reaction of rPrP into the amyloid fibrils involves multiplication of active centers through fibril fragmentation and quenching of active centers.

apparent volume-dependent threshold effect; and (5) the lack of effect the amount of seeds has on the rate of seeded conversion. These kinetic features are not typical for the polymerization kinetics displayed by other amyloidogenic proteins and could not be explained by simple NPM.

To explain the distinctive kinetic behavior of rPrP polymerization, we applied a more complex model of nucleation−polymerization introduced recently in several studies (*48*−*50*). According to this model, in addition to the steps of nucleation and elongation, the polymerization of rPrP in vitro involves multiplication of active centers of polymerization (Figure 8). Recent work by Weissman and co-workers (*41*) demonstrated that the multiplication of active centers during polymerization of the yeast prion protein Sup 35 occurs through fibril fragmentation. Our observation that a substantial subpopulation of rPrP fibrils remained short even by the end of the elongation stage is consistent with the new model that postulates fibril fragmentation as an important step of in vitro conversion (Figure 6). Although we were not able to measure directly the fragmentation of fibrils in solution, electron microscopy of individual fibrils illustrated the potential fragility of amyloid structures (Figure 7).

Remarkably, addition of a fragmentation step to NPM not only explains the strongly sigmoidal shape of the kinetic curve but also could account for the reduced concentration dependence of the length of the lag phase, the feature that otherwise would be difficult to explain within a simple NPM framework (*41*, *50*). According to simple NPM, formation of oligomeric nucleus is controlled by the mass-action law; therefore, the length of the lag phase is expected to depend strongly on protein concentration. However, when a fragmentation step is incorporated into NPM, modeling of polymerization kinetics was shown to give only a first-order dependence of the lag phase on protein concentration for a nucleus size of six, and this dependence decreased even further for smaller nucleus size (*41*). Therefore, the weak dependence of the lag phase on the concentration of rPrP observed in the present studies can be rationalized by the model that incorporates multiplication of active centers during polymerization (Figure 8). It is quite likely that the combination of partially denaturing conditions and shaking employed in the present conversion protocol is necessary for fibril fragmentation. An alternative in vitro conversion protocol developed for amplification of PK-resistant PrP^{Sc}-like isoforms required repetitive cycles of sonication, which are also believed to result in fragmentation of PrP^{Sc} aggregates (*51*). While fragmentation of yeast prion aggregates seems to involve cellular chaperones (*52*, *53*), the mechanism responsible for multiplication of catalytic centers of PrP^{Sc} in vivo is currently unknown. Nevertheless, the ability to

control multiplication of the catalytic isoform of PrP would be a powerful strategy to treat prion diseases.

Other unusual kinetic features observed in the present studies involve an apparent first-order rate of polymerization and lack of dependence of the rate of seeded conversion on the amount of seeds. The first-order rate of polymerization is in agreement with a proposition that it is postbinding events, such as a conformational rearrangement, rather than binding of rPrP polypeptides to growing fibrils that determines the rate-limiting step of polymerization (Figure 8). On the other hand, if one considers postbinding rearrangement as a sole rate-limiting step, it would be difficult to explain why the amount of seeds used for the seeded polymerization does not affect the rate of polymerization but only the length of the lag phase (Figure 5). Fibril fragmentation is another elementary step that follows apparent first-order kinetics and could be a critical rate-limiting step (Figure 8). If the fibril fragmentation occurs in parallel with elongation, then at a given concentration of rPrP, the polymerization rate measured by ThT assay will be a function of both intrinsic fibril fragility and the rate of postbinding rearrangement rather than the initial amount of seeds. If fibrils do not undergo fragmentation, then the amount of active centers of polymerization would remain constant during the entire conversion reaction, and therefore the rate of polymerization would be proportional to the amount of initial seeds (Figure 5B). In our experiment, the rate of polymerization was constant (Figure 5A).

While detailed effects of fibril fragmentation on kinetics of polymerization remains to be established in future studies, by incorporating a fragmentation step into NPM we can explain several otherwise puzzling features of rPrP polymerization observed here. Notably, if the intrinsic fragility of PrP^{Sc} aggregates does dictate the rate of prion propagation, this property could account for substantial differences in the incubation times produces by different strains of PrP^{Sc} (*13*).

While multiplication of active centers helps to rationalize several atypical kinetic features, the threshold effect has not yet been explained. This effect could be in part due to lower effectiveness of shaking at volumes below 0.3 mL. Specifically, the rate of fragmentation might drop substantially at volumes below 0.3 mL due to less effective shaking. Within the detection limit of the ThT binding assay, we were unable to detect any amyloid fibrils in the reaction volume below 0.3 mL. Even if a residual amount of amyloid fibrils is produced in small volumes, their active concentration in solution may not increase at all due to ongoing sorption of fibrils to walls of the reaction vessels. We found that amyloid fibrils had high propensity for sorption to surfaces, a process that may counteract production of fibrils in solution. Because sorption of fibrils is surface-dependent, the surface-to-volume ratio could be another factor that determines apparent volume-dependent threshold effect.

Taken together, our findings are consistent with the NPM in which the polymerization reaction is regulated by the fine balance between two processes: multiplication and deactivation of active centers. In its new format, the NPM predict that this balance has a dramatic effect on the final outcome of the in vitro conversion reaction or progression of prion disease in vivo. When multiplication of the active centers exceeds their quenching, the conversion reaction proceeds with self-acceleration. If the rate of quenching is higher than the rate of multiplication, the reaction decays, a kinetic parameter that explains subthreshold conditions. Correspondingly, it is expected that PrP^{Sc} will be cleared throughout an animal's lifetime if the process of prion replication is slower than the clearance. When the rate of multiplication is balanced with the rate of deactivation, apparently negligible changes in experimental parameters may switch the reaction from decay mode to autoacceleration mode and vice versa, causing stochastic behavior, in which the reaction follows the "all or nothing" rule.

The model in which the fine balance between multiplication and clearance of PrP^{Sc} determines progression of prion disease is consistent with several experimental observations. For example, the concentration of PrP^{Sc} in the brain of experimental animals drops substantially in the first week after intracerebral inoculation (*54*, *55*), illustrating that the rate of clearance exceeds the rate of multiplication during the initial stage of prion transmission. Surprisingly, the lifetime of PrP^{Sc} was found to be relatively short despite substantial resistance to proteolytic digestion (*56*, *57*). Under conditions that inhibit production of nascent PrP^{Sc}, the half-life of PrP^{Sc} in ScN2a cells was shown to be only 28 h (*56*). Multiple factors may influence the rate of clearance of PrP^{Sc} in vivo: strain-specific intrinsic stability of PrP^{Sc} (*13*, *58*), intensity of proteolytic processing (*59*, *60*), and interaction of PrP^{Sc} with stabilizing cofactors such as glycosaminoglycans (*61*−*63*). Our data indicate that sorption of self-propagating amyloid isoform to walls of reaction vessels may account for deactivation. Although sorption of the amyloid fibrils seems to be a peculiar feature of the conversion in vitro, it may, in fact, mimic the clearance of the PrP^{Sc} form in vivo and thus provide insight into the underlying mechanisms of prion replication.

In the present studies we demonstrate that full-length rPrP has a remarkably high intrinsic propensity to convert into the amyloid form. The in vitro conversion of rPrP occurs at concentration of 0.22 μM, which is below that found in a cell (*12*). Most in vitro conversion reactions by other amyloidogenic proteins and PrP-derived polypeptides that undergo nucleation-dependent conversion require amounts 100−2000-fold higher than those reported in the present study. For comparison, the amyloidogenic concentration of PrP-derived polypeptide encompassing residues 23−144 was 2000-fold higher than that used here for full-length rPrP (*31*). This result indicates that full-length PrP possesses the unique ability to adopt an amyloid-specific conformation, and that this ability may not be well preserved by smaller peptides such as PrP 23−144. Notably, the recent studies with molecular dynamic simulations demonstrated that the region corresponding to helices B and C (residues 170−230) seems to play a central role in the initial stages of conformational transitions from α-helical to β-sheet-rich conformation (*64*).

In the present study we showed that the conversion of rPrP into fibrillar form displays a dramatic volume-dependent threshold effect. In contrast to the amyloid formation, the generation of another β-sheet-rich isoform of rPrP, referred to as β-oligomer, was highly concentration-dependent but independent of the reaction volume. Taken together, our study illustrates that the reaction volume is one of the experimental factors that may discriminate between the two routes of in vitro conversion: formation of fibrils versus the β-oligomer. Notably, apparent volume-dependent threshold

effects may account in part for technical difficulties in generation of amyloid fibrils and confusion between different β-sheet-rich isoforms of rPrP reported in previous studies.

ACKNOWLEDGMENT

We thank Sylvain Lehmann for providing PrP plasmids, Alexander Parfenov for taking fluorescent images, and Vadim Salnikov for taking electron microscopic images.

REFERENCES

1. Prusiner, S. B. (1982) Novel proteinaceous infectious particles cause scrapie, *Science 216*, 136−144.
2. Pan, K.-M., Baldwin, M., Nguyen, J., Gasset, M., Serban, A., Groth, D., Mehlhorn, I., Huang, Z., Fletterick, R. J., Cohen, F. E., and Prusiner, S. B. (1993) Conversion of α-helices into β-sheets features in the formation of the scrapie prion proteins, *Proc. Natl. Acad. Sci. U.S.A. 90*, 10962−10966.
3. Caughey, B. W., Dong, A., Bhat, K. S., Ernst, D., Hayes, S. F., and Caughey, W. S. (1991) Secondary structure analysis of the scrapie-associated protein PrP 27−30 in water by infrared spectroscopy, *Biochemistry 30*, 7672−7680.
4. Lasmézas, C. I., Deslys, J.-P., Robain, O., Jaegly, A., Beringue, V., Peyrin, J.-M., Fournier, J.-G., Hauw, J.-J., Rossier, J., and Dormont, D. (1997) Transmission of the BSE agent to mice in the absence of detectable abnormal prion protein, *Science 275*, 402−405.
5. Manuelidis, L., Fritch, W., and Xi, Y.-G. (1997) Evolution of a strain of CJD that induces BSE-like plaques, *Science 277*, 94−98.
6. Barron, R. M., Thomson, V., Jameison, E., Melton, D. W., Ironside, J., Will, R., and Manson, J. C. (2001) Changing a single amino acid in the N-terminus of murine PrP alters TSE incubation time across three species barrier, *EMBO J. 20*, 5070−5078.
7. Bieschke, J., Weber, P., Sarafoff, N., Beekes, M., Giese, A., and Kretzschmar, H. (2004) Autocatalytic self-propagation of misfolded prion protein, *Proc. Acad. Natl. Sci. U.S.A. 101*, 12207−12211.
8. Jackson, G. S., Hosszu, L. L. P., Power, A., Hill, A. F., Kenney, J., Saibil, H., Craven, C. J., Waltho, J. P., Clarke, A. R., and Collinge, J. (1999) Reversible conversion of monomeric human prion protein between native and fibrilogenic conformations, *Science 283*, 1935−1937.
9. Hill, A. F., Antoniou, M., and Collinge, J. (1999) Protease-resistant prion protein produced in vitro lacks detectable infectivity, *J. Gen. Virol. 80*, 11−14.
10. Bessen, R. A., and Marsh, R. F. (1994) Distinct PrP properties suggest the molecular basis of strain variation in transmissible mink encephalopathy, *J. Virol. 68*, 7859−7868.
11. Telling, G. C., Parchi, P., DeArmond, S. J., Cortelli, P., Montagna, P., Gabizon, R., Mastrianni, J., Lugaresi, E., Gambetti, P., and Prusiner, S. B. (1996) Evidence for the conformation of the pathologic isoform of the prion protein enciphering and propagating prion diversity, *Science 274*, 2079−2082.
12. Safar, J., Wille, H., Itri, V., Groth, D., Serban, H., Torchia, M., Cohen, F. E., and Prusiner, S. B. (1998) Eight prion strains have PrP^{Sc} molecules with different conformations, *Nat. Med. 4*, 1157−1165.
13. Peretz, D., Scott, M., Groth, D., Williamson, A., Burton, D., Cohen, F. E., and Prusiner, S. B. (2001) Strain-specified relative conformational stability of the scrapie prion protein, *Protein Sci. 10*, 854−863.
14. Caughey, B., Raymond, G. J., and Bessen, R. A. (1998) Strain-dependent differences in β-sheet conformations of abnormal prion protein, *J. Biol. Chem. 273*, 32230−32235.
15. Hill, A. F., Joiner, S., Wadsworth, J. D. F., Sidle, K. C. L., Bell, J. E., Budka, H., Ironside, J. W., and Collinge, J. (2003) Molecular classification of sporadic Creutzfeldt-Jakob disease, *Brain 126*, 1333−1346.
16. Parchi, P., Giese, A., Capellari, S., Brown, P., Schulz-Schaeffer, W., Windl, O., Zerr, I., Budka, H., Kopp, N., Piccardo, P., Poser, S., Rojiani, A., Streichemberger, N., Julien, J., Vital, C., Ghetti, B., Gambetti, P., and Kretzschmar, H. (1999) Classification of sporadic Creutzfeldt-Jakob disease based on molecular and phenotypic analysis of 300 subjects, *Ann. Neurol. 46*, 224−233.
17. Baskakov, I. V., Legname, G., Prusiner, S. B., and Cohen, F. E. (2001) Folding of prion protein to its native α-helical conformation is under kinetic control, *J. Biol. Chem. 276*, 19687−19690.
18. Rezaei, H., Choiset, Y., Eghiaian, F., Treguer, E., Mentre, P., Debey, P., Grosclaude, J., and Haertle, T. (2002) Amyloidogenic Unfolding Intermediates Differentiate Sheep Prion Protein Variants, *J. Mol. Biol. 322*, 799−814.
19. Lee, S., and Eisenberg, D. (2003) Seeded conversion of recombinant prion protein to a disulfide-bonded oligomer by a reduction−oxidation process, *Nat. Struct. Biol. 10*, 725−730.
20. Kazlauskaite, J., Sanghera, N., Sylvester, I., Venien-Bryan, C., and Pinheiro, T. J. (2003) Structural changes of the prion protein in lipid membranes leading to aggregation and fibrillization, *Biochemistry 42*, 3295−3304.
21. Sokolowski, F., Modler, A. J., Masuch, R., Zirwer, D., Baier, M., Lutsch, G., Moss, D. A., Gast, K., and Naumann, D. (2003) Formation of critical oligomers is a key event during conformational transition of recombinant syrian hamster prion protein, *J. Biol. Chem. 278*, 40481−40492.
22. Torrent, J., Alvarez-Martinez, M. T., Heitz, F., Liautard, J. P., Balny, C., and Lange, R. (2003) Alternative Prion Structural changes Revealed by High Pressure, *Biochemistry 42*, 1318−1325.
23. Cordeiro, Y., Machado, F., Juliano, L., Juliano, M. A., Brentani, R. R., Foguel, D., and Silva, J. L. (2001) DNA Converts Cellular Prion Protein into the beta-Sheet Conformation and Inhibits Prion Peptide Aggregation, *J. Biol. Chem. 276*, 49400−49409.
24. Swietnicki, W., Morillas, M., Chen, S. G., Gambetti, P., and Surewicz, W. K. (2000) Aggregation and fibrillization of the recombinant human prion protein huPrP90−231, *Biochemistry 39*, 424−431.
25. May, B. C. H., Govaerts, C., Prusiner, S. B., and Cohen, F. E. (2004) Prions: so many fibers, so little infectivity, *Trends Biochem. Sci. 29*, 162−165.
26. Baskakov, I. V., Legname, G., Baldwin, M. A., Prusiner, S. B., and Cohen, F. E. (2002) Pathway Complexity of Prion Protein Assembly into Amyloid, *J Biol. Chem. 277*, 21140−21148.
27. Baskakov, I. V. (2004) Autocatalytic conversion of Recombinant Prion Proteins Displays a Species Barrier, *J Biol. Chem. 279*, 586−595.
28. Legname, G., Baskakov, I. V., Nguyen, H.-O. B., Riesner, D., Cohen, F. E., DeArmond, S. J., and Prusiner, S. B. (2004) Synthetic mammalian prions, *Science 305*, 673−676.
29. Harper, J. D., and Lansbury, P. T., Jr. (1997) Models of amyloid seeding in Alzheimer's disease and scrapie: mechanistic truths and physiological consequences of the time-dependent solubility of amyloid proteins, *Annu. Rev. Biochem. 66*, 385−407.
30. Oosawa, F., and Asakura, S. (1975) *Thermodynamics of Polymerization of Protein*, Academic Press, London.
31. Kundu, B., Maiti, N. R., Jones, E. M., Surewicz, K. A., Vanik, D. L., and Surewicz, W. K. (2003) Nucleation-dependent conformational conversion of the Y145Stop variant of human prion protein: Structural clues for prion propagation, *Proc. Acad. Natl. Sci. U.S.A. 100*, 12069−12074.
32. Padrick, S. P., and Miranker, A. D. (2002) Islet Amyloid: Phase Partitioning and Secondary Nucleation Are Central to the Mechanism of Fibrillogenesis, *Biochemistry 41*, 4694−4703.
33. Chen, S., Ferrone, F. A., and Wetzel, R. (2002) Huntington's disease age-of-onset linked to polyglutamine aggregation nucleation, *Proc. Acad. Natl. Sci. U.S.A. 99*, 11884−11889.
34. Baskakov, I. V., Aagaard, C., Mehlhorn, I., Wille, H., Groth, D., Baldwin, M. A., Prusiner, S. B., and Cohen, F. E. (2000) Self-assembly of recombinant prion protein of 106 residues, *Biochemistry 39*, 2792−2804.
35. Hamada, D., and Dobson, C. M. (2002) A kinetic of beta-lactoglobulin amyloid fibril formation promoted by urea, *Protein. Sci. 11*, 2417−2426.
36. Weissmann, C. (2004) The state of the prion, *Nat. Rev. Microbiol. 2*, 861−871.
37. Rhoades, E., and Gafni, A. (2003) Micelle Formation by a Fragment of Human Islet Amyloid Polypeptide, *Biophys. J. 84*, 3480−3487.
38. Souillac, P. O., Uversky, V. N., and Fink, A. L. (2003) Structural Transformations of Oligomeric Intermediates in the Fibrillation of the Immunoglobulin Light Chain LEN, *Biochemistry 42*, 8094−8104.
39. Zahn, R. (2003) The Octapeptide Repeats in Mammalian Prion Protein Constitue a pH-dependent Folding and Aggregation Site, *J. Mol. Biol. 334*, 477−488.

40. Vanik, D. L., Surewicz, K. A., and Surewicz, W. K. (2004) Molecular Basis of Barriers for Interspecies Transmissibility of Mammalian Prions, *Mol. Cell 14*, 139−145.
41. Collins, S. R., Douglass, A., Vale, R. D., and Weissman, J. S. (2004) Mechanism of Prion Propagation: Amyloid Growth Occurs by Monomer Addition, *PLOS Biol. 2*, e321.
42. Zhu, M., Souillac, P. O., Ionescu-Zanetti, C., Carter, S. A., and Fink, A. L. (2002) Surface-catalyzed Amyloid Fibril Formation, *J. Biol. Chem. 277*, 50914−50922.
43. Klunk, W. E., Jacob, R. F., and Mason, R. P. (1999) Quantifying amyloid by congo red spectral shift assay, *Methods Enzymol. 309*, 285−305.
44. Bernouilli, C., Siegfried, J., Baumgartner, G., Regli, F., Rabinowicz, T., Gajdusek, D. C., and Gibbs, C. J., Jr. (1977) Danger of accidental person to person transmission of Creutzfeldt-Jakob disease by surgery, *Lancet 1*, 478−479.
45. Gibbs, C. J., Jr., Asher, D. M., Kobrine, A., Amyx, H. L., Sulima, M. P., and Gajdusek, D. C. (1994) Transmission of Creutzfeldt-Jakob disease to a chimpanzee by electrodes contaminated during neurosurgery, *J. Neurol. Neurosurg. Psychiatry 57*, 757−758.
46. Zobeley, E., Flechsig, E., Cozzio, A., Enari, M., and Weissmann, C. (1999) Infectivity of scrapie prions bound to a stainless steel surface, *Mol. Med. 5*, 240−243.
47. Weissmann, C., Enari, M., Klohn, P. C., Rossi, D., and Flechsig, E. (2002) Transmission of Prions, *J. Infect. Dis. 186* (Suppl. 2), S157−S165.
48. Poschel, T., Brilliantov, N. V., and Frommel, C. (2003) Kinetics of Prion Growth, *Biophys. J. 85*, 3460−3474.
49. Masel, J., Jansen, V. A. A., and Nowak, M. A. (1999) Quantifying the kinetic parameters of prion replication, *Biophys. Chem. 77*, 139−152.
50. Ferrone, F. (1999) Analysis of protein aggregation kinetics, *Methods Enzymol. 309*, 256−274.
51. Saborio, G. P., Permanne, B., and Soto, C. (2001) Sensitive detection of pathological prion protein by cyclic amplification of protein misfolding, *Nature 411*, 810−813.
52. Ness, F., Ferreira, P., Cox, B. S., and Tuite, M. F. (2002) Guanidine hydrochloride inhibits the generation of prion "seeds" but not prion protein aggregation in yeast, *Mol Cell. Biol. 22*, 5593−5605.
53. Osherovich, L. Z., Cox, B. S., Tuite, M. F., and Weissman, J. S. (2004) Dissection and design of yeast prions, *PLoS Biol. 2*, e86.
54. Bolton, D. C., Seligman, S. J., Bablanian, G., Windsor, D., Scala, L. J., Kim, K. S., Chen, C. J., Kascsak, R. J., and Bendheim, P. E. (1991) Molecular location of a species-specific epitope on the hamster scrapie agent protein, *J. Virol. 65*, 3667−3675.
55. Bueler, H., Aguzzi, A., Sailer, A., Greiner, R. A., Autenried, P., Aguet, M., and Weissmann, C. (1993) Mice Devoid of PrP are Resistant to Scrapie, *Cell 73*, 1339−1347.
56. Peretz, D., Williamson, R. A., Kaneko, K., Vergara, J., Leclerc, E., Schmitt-Ulms, G., Mehlhorn, I. R., Legname, G., Wormald, M. R., Rudd, P. M., Dwek, R. A., Burton, D. R., and Prusiner, S. B. (2001) Antibodies inhibit prion propagation and clear cell cultures of prion infectivity, *Nature 412*, 739−743.
57. Enari, M., Flechsig, E., and Weissmann, C. (2001) Scrapie prion protein accuulation by scrapie-infected neuroblastoma cells abrogated by exosure to a prion protein antibody, *Proc. Acad. Natl. Sci. U.S.A. 98*, 9295−9299.
58. Kuczius, T., and Groschup, M. H. (1999) Differences in Proteinase K Resistance and Neuronal Deposition of Abnormal Prion Proteins Characterize Bovine Spongioform Encephalopathy (BSE) and Scrapie Strains, *Mol. Med. 5*, 406−418.
59. Luhr, K. M., Nordstromm, E. K., Low, P., Ljunggren, H. G., Taraboulos, A., and Kristensson, K. (2004) Scrapie Protein Degradation by Cysteine Protease in CD11c+ Dendritic Cells and GT1-1 Neuronal Cells, *J. Virol. 78*, 4776−4782.
60. Yadavalli, R., Guttmann, R. P., Seward, T., Centers, A. P., Williamson, R. A., and Telling, G. C. (2004) Calpain-dependent endoproteolytic cleavage of PrPSc modulates scrapie prion, *J. Biol. Chem. 279*, 21948−21956.
61. Wong, C., Xiong, L. W., Horiuchi, M., Raymond, L., Wehrly, K., Chesebro, B., and Caughey, B. (2001) Sulfated glycans and elevated temperature stimulate PrP(Sc)-dependent cell-free formation of protease-resistant prion protein, *EMBO J., 20*, 377−386.
62. Shaked, G. M., Meiner, Z., Avraham, I., Taraboulos, A., and Gabizon, R. (2001) Reconstitution of Prion Infectivity from Solubilized Protease-resistant PrP and Nonprotein Components of Prion Rods, *J. Biol. Chem. 276*, 14324−14328.
63. Ben-Zaken, O., Tzaban, S., Tal, Y., Horonchik, L., Esko, J. D., Vlodavsky, I., and Taraboulos, A. (2003) Cellular Heparan Sulfate Participates in the Metabolism of Prions, *J. Biol. Chem. 41*, 40041−40049.
64. Dima, R. I., and Thirumalai, D. (2004) Probing the instabilities in the dynamics of helical fragments from mouse PrPC, *Proc. Natl. Acad. Sci. U.S.A. 101*, 15335−15340.
65. Baskakov, I. V., Legname, G., Gryczynski, Z., and Prusiner, S. B. (2004) The peculiar nature of unfolding of human prion protein, *Protein Sci. 13*, 586−595.

BI048322T